Science Advances
AAAS
Manuscript

Oxygen isotopes of anhydrous primary minerals show kinship between asteroid Ryugu and comet 81P/Wild2

Short title: Oxygen isotopes of Ryugu primary minerals

Noriyuki Kawasaki[1]*, Kazuhide Nagashima[2], Naoya Sakamoto[3], Toru Matsumoto[4,5], Ken-ichi Bajo[1], Sohei Wada[1], Yohei Igami[5], Akira Miyake[5], Takaaki Noguchi[5], Daiki Yamamoto[6], Sara S. Russell[7], Yoshinari Abe[8], Jérôme Aléon[9], Conel M. O'D. Alexander[10], Sachiko Amari[11,12], Yuri Amelin[13], Martin Bizzarro[14], Audrey Bouvier[15], Richard W. Carlson[10], Marc Chaussidon[16], Byeon-Gak Choi[17], Nicolas Dauphas[18], Andrew M. Davis[18], Tommaso Di Rocco[19], Wataru Fujiya[20], Ryota Fukai[21], Ikshu Gautam[6], Makiko K. Haba[6], Yuki Hibiya[22], Hiroshi Hidaka[23], Hisashi Homma[24], Peter Hoppe[25], Gary R. Huss[2], Kiyohiro Ichida[26], Tsuyoshi Iizuka[27], Trevor R. Ireland[28], Akira Ishikawa[6], Motoo Ito[29], Shoichi Itoh[5], Noriko T. Kita[30], Kouki Kitajima[30], Thorsten Kleine[31], Shintaro Komatani[26], Alexander N. Krot[2], Ming-Chang Liu[32], Yuki Masuda[6], Kevin D. McKeegan[32], Mayu Morita[26], Kazuko Motomura[33], Frédéric Moynier[16], Izumi Nakai[34], Ann Nguyen[35], Larry Nittler[10], Morihiko Onose[26], Andreas Pack[19], Changkun Park[36], Laurette Piani[37], Liping Qin[38], Maria Schönbächler[39], Lauren Tafla[32], Haolan Tang[32], Kentaro Terada[40], Yasuko Terada[41], Tomohiro Usui[20], Meenakshi Wadhwa[42], Richard J. Walker[43], Katsuyuki Yamashita[44], Qing-Zhu Yin[45], Tetsuya Yokoyama[6], Shigekazu Yoneda[46], Edward D. Young[32], Hiroharu Yui[47], Ai-Cheng Zhang[48], Tomoki Nakamura[49], Hiroshi Naraoka[50], Ryuji Okazaki[50], Kanako Sakamoto[21], Hikaru Yabuta[51], Masanao Abe[21], Akiko Miyazaki[21], Aiko Nakato[21], Masahiro Nishimura[21], Tatsuaki Okada[21], Toru Yada[21], Kasumi Yogata[21], Satoru Nakazawa[21], Takanao Saiki[21], Satoshi Tanaka[21], Fuyuto Terui[52], Yuichi Tsuda[21], Sei-ichiro Watanabe[23], Makoto Yoshikawa[21], Shogo Tachibana[53], Hisayoshi Yurimoto[1,3]

Affiliations:

[1]Department of Natural History Sciences, Hokkaido University; Sapporo 060-0810, Japan.

[2]Hawai‘i Institute of Geophysics and Planetology, University of Hawai‘i at Mānoa; Honolulu, HI 96822, USA.

[3]Isotope Imaging Laboratory, Creative Research Institution, Hokkaido University; Sapporo 001-0021, Japan.

[4]The Hakubi Center for Advanced Research, Kyoto University; Kitashirakawaoiwake-cho, Sakyo-ku, Kyoto 606-8502, Japan.

[5]Division of Earth and Planetary Sciences, Kyoto University; Kitashirakawaoiwake-cho, Sakyo-ku, Kyoto 606-8502, Japan.

[6]Department of Earth and Planetary Sciences, Tokyo Institute of Technology; Tokyo 152-8551, Japan.

[7]Department of Earth Sciences, Natural History Museum; London, SW7 5BD, UK.

[8]Graduate School of Engineering Materials Science and Engineering, Tokyo Denki University; Tokyo 120-8551, Japan.

[9]Institut de Minéralogie, de Physique des Matériaux et de Cosmochimie, Sorbonne Université, Museum National d'Histoire Naturelle, Centre National de la Recherche Scientifique Unité Mixte de Recherche 7590, IRD; 75005 Paris, France.

[10]Earth and Planets Laboratory, Carnegie Institution for Science; Washington, DC, 20015, USA.

[11]McDonnell Center for the Space Sciences and Physics Department, Washington University; St. Louis, MO 63130, USA.

[12]Geochemical Research Center, The University of Tokyo, Tokyo, 113-0033, Japan.

[13]Guangzhou Institute of Geochemistry, Chinese Academy of Sciences; Guangzhou, GD 510640, China.

[14]Centre for Star and Planet Formation, Globe Institute, University of Copenhagen; Copenhagen, K 1350, Denmark.

[15]Bayerisches Geoinstitut, Universität Bayreuth; Bayreuth 95447, Germany.

[16]Université de Paris, Institut de physique du globe de Paris, Centre National de la Recherche Scientifique; 75005 Paris, France.

[17]Department of Earth Science Education, Seoul National University; Seoul 08826, Republic of Korea.

[18]Department of the Geophysical Sciences and Enrico Fermi Institute, The University of Chicago; Chicago, IL 60637, USA.

[19]Faculty of Geosciences and Geography, University of Göttingen; Göttingen, D-37077, Germany.

[20]Faculty of Science, Ibaraki University; Mito 310-8512, Japan.

[21]Institute of Space and Astronautical Science, Japan Aerospace Exploration Agency; Sagamihara 252-5210, Japan.

[22]General Systems Studies, The University of Tokyo; Tokyo 153-0041, Japan.

[23]Earth and Planetary Sciences, Nagoya University; Nagoya 464-8601, Japan.

[24]Osaka Application Laboratory, Rigaku Corporation; Osaka 569-1146, Japan.

[25]Max Planck Institute for Chemistry; Mainz 55128, Germany.

[26]Analytical Technology, Horiba Techno Service Co., Ltd.; Kyoto 601-8125, Japan.

[27]Earth and Planetary Science, The University of Tokyo; Tokyo 113-0033, Japan.

[28]School of Earth and Environmental Sciences, The University of Queensland; St Lucia QLD 4072, Australia.

[29]Kochi Institute for Core Sample Research, Japan Agency for Marine-Earth Science and Technology; Kochi 783-8502, Japan.

[30]Geoscience, University of Wisconsin- Madison; Madison, WI 53706, USA.

[31]Max Planck Institute for Solar System Research; 37077 Göttingen, Germany.

[32]Earth, Planetary, and Space Sciences, University of California, Los Angeles; Los Angeles, CA 90095, USA.

[33]Thermal Analysis, Rigaku Corporation; Tokyo 196-8666, Japan.

[34]Applied Chemistry, Tokyo University of Science; Tokyo 162-8601, Japan.

[35]Astromaterials Research and Exploration Science Division, National Aeronautics and Space Administration Johnson Space Center; Houston, TX 77058, USA.

[36]Earth-System Sciences, Korea Polar Research Institute; Incheon 21990, Korea.

[37]Centre de Recherches Pétrographiques et Géochimiques, Centre National de la Recherche Scientifique - Université de Lorraine; 54500 Nancy, France.

[38]University of Science and Technology of China, School of Earth and Space Sciences; Anhui 230026, China.

[39]Institute for Geochemistry and Petrology, Department of Earth Sciences, Eidgenössische Technische Hochschule Zürich; Zürich, Switzerland.

[40]Earth and Space Science, Osaka University; Osaka 560-0043, Japan.

[41]Spectroscopy and Imaging, Japan Synchrotron Radiation Research Institute; Hyogo 679-5198 Japan.

[42]School of Earth and Space Exploration, Arizona State University; Tempe, AZ 85281, USA.

[43]Geology, University of Maryland, College Park, MD 20742, USA.

[44]Graduate School of Natural Science and Technology, Okayama University; Okayama 700-8530, Japan.

[45]Earth and Planetary Sciences, University of California; Davis, CA 95616, USA.

[46]Science and Engineering, National Museum of Nature and Science; Tsukuba 305-0005, Japan.

[47]Chemistry, Tokyo University of Science; Tokyo 162-8601, Japan.

[48]School of Earth Sciences and Engineering, Nanjing University; Nanjing 210023, China.

[49]Department of Earth Science, Tohoku University; Sendai, 980-8578, Japan.

[50]Department of Earth and Planetary Sciences, Kyushu University; Fukuoka 819-0395, Japan.

[51]Earth and Planetary Systems Science Program, Hiroshima University; Higashi-Hiroshima, 739-8526, Japan.

[52]Kanagawa Institute of Technology; Atsugi 243-0292, Japan.

[53]UTokyo Organization for Planetary and Space Science, University of Tokyo; Tokyo 113-0033, Japan.

*Corresponding author. Email: kawasaki@ep.sci.hokudai.ac.jp

Abstract:

The extraterrestrial materials returned from asteroid (162173) Ryugu consist predominantly of low-temperature aqueously formed secondary minerals and are chemically and mineralogically similar to CI (Ivuna-type) carbonaceous chondrites. Here we show that high-temperature anhydrous primary minerals in Ryugu and CI chondrites exhibit a bimodal distribution of oxygen isotopic compositions: ^{16}O-rich (associated with refractory inclusions) and ^{16}O-poor (associated with chondrules). Both the ^{16}O-rich and ^{16}O-poor minerals probably formed in the inner solar protoplanetary disk and were subsequently transported outwards. The abundance ratios of the ^{16}O-rich to ^{16}O-poor minerals in Ryugu and CI chondrites are higher than in other carbonaceous chondrite groups, but are similar to that of comet 81P/Wild2, suggesting that Ryugu and CI chondrites accreted in the outer Solar System closer to the accretion region of comets.

(126 words)

Teaser

C-type asteroid Ryugu formed in the outer Solar System close to the accretion region of 81P/Wild2 comet.

(104 characters)

MAIN TEXT:

Introduction

Samples returned from asteroid (162173) Ryugu by the JAXA Hayabusa2 spacecraft (*1*) have mineralogical, petrological, and chemical characteristics similar to those of CI (Ivuna-type) carbonaceous chondrites (*2, 3*). The Ryugu samples and CI chondrites consist mainly of secondary minerals (phyllosilicates, carbonates, magnetite, and pyrrhotite) aqueously altered from anhydrous primary minerals in their parent bodies at low-temperature. High-temperature anhydrous primary minerals, including olivine, low-Ca pyroxene, spinel, hibonite, and perovskite, are rare (*2–8*). Most primary phases in Ryugu and CI chondrites are small (< ~20 μm) and monomineralic (*5*), providing little information on their origin. The morphology and chemical compositions of olivine grains in Ryugu (*2*) and CI chondrites (*4, 6*) are consistent with originating as chondrule phenocrysts. A porous olivine-diopside object in Ryugu (*2, 9*) could be genetically related to amoeboid olivine aggregates (AOAs), a common type of refractory inclusions observed in chondrites (*10*).

Oxygen isotopic compositions of primary minerals can potentially provide important constraints on their origin. In carbonaceous chondrites, the O isotopic compositions of minerals in chondrules and refractory inclusions [AOAs and Ca-Al-rich inclusions (CAIs)] show a bimodal distribution of $\Delta^{17}O$, deviation from terrestrial mass-dependent fractionation law ($= \delta^{17}O - 0.52\times\delta^{18}O$, where $\delta^{i}O = [(^{i}O/^{16}O)_{sample}/(^{i}O/^{16}O)_{SMOW} - 1] \times 1000$, i = 17 or 18, and SMOW is standard mean ocean water) (*11, 12*). Most refractory inclusions have solar-like ^{16}O-rich compositions with $\Delta^{17}O \sim -23‰$ (*12*), while chondrules are ^{16}O-depleted to various degrees with $\Delta^{17}O$ values that range from ~ −7‰ to ~ 0‰ (Fig. 1, A to D) (*13–17*).

The previously reported O isotopic compositions of olivine and low-Ca pyroxene grains separated from CI chondrites (*4, 6*) show $\Delta^{17}O$ values that range from ~ −6 to +3‰ with a clear mode in the distribution at ~ 0‰ (Fig. 1E), which is different from the modes of olivine and low-Ca pyroxene chondrule phenocrysts in other carbonaceous chondrites, at ~ −6 and ~ −2‰, respectively (Fig. 1, A to D) (*13–17*). The O isotopic compositions of olivine and low-Ca pyroxene grains embedded in matrices of CI chondrites were measured *in situ* (*7*). The data of ^{16}O-poor grains follow a near-uniform distribution ranging between $\Delta^{17}O \sim -7$ and −1‰ without any distinct peak (Fig. 1F). So far, no clear evidence for the genetic relationship between olivine and low-Ca pyroxene grains of CI and chondrule minerals of carbonaceous chondrites has been established. Some ^{16}O-rich ($\Delta^{17}O \sim -20‰$) olivine and low-Ca pyroxene grains were observed in CI chondrites and Ryugu samples (Fig. 1, F and G), possibly related to AOAs (*7–9*). Here, we report O isotopic compositions of primary minerals (olivine, low-Ca pyroxene, and spinel) measured *in situ* in polished sections of Ryugu and Ivuna, and we identify the first unambiguous AOA object in CI chondrites. We also discuss the implications of these data for understanding (*i*) the origin of anhydrous primary minerals in Ryugu and CIs, (*ii*) the genetic relationship between Ryugu and CI chondrites, and (*iii*) the accretion region of Ryugu and CI chondrite parent bodies.

Results

Primary minerals, like olivine, low-Ca pyroxene, and spinel, are rare in the Ryugu and Ivuna samples studied, consistent with the previous studies (*2, 5*). They occur primarily in ~100–500 μm-sized clasts enriched in S and Fe and depleted in Mg and Si compared to major lithologies of Ryugu (Fig. 2 and fig. S1 to S3) and Ivuna (fig. S4 and S5). Different chemical compositions of the less-altered clasts from major lithologies may be due to difference in chemical compositions of aqueous fluids (*2*). The anhydrous primary minerals are embedded in hydrated matrix composed of phyllosilicates (serpentine and saponite) and coarser-grained magnetite, sulfides, and carbonates

(Fig. 2 and fig. S6 to S8). The carbonates are almost exclusively calcite; dolomite and breunnerite, commonly observed in the main lithologies of Ryugu and Ivuna, are nearly absent in the Fe-rich clasts. Most olivine grains are irregularly shaped fragments with sizes up to ~15 μm in Ryugu and up to ~30 μm in Ivuna. The chemical compositions of the olivine grains range from Mg# (= Mg/(Mg+Fe)×100) ~57 to ~99, but the very Mg-rich olivine grains (Mg# > 97) are dominant (fig. S9).

A Ryugu piece from the first touchdown site (A104-009008) contains anhydrous primary minerals of olivine and Mg-Al spinel. The other minerals included in the piece are mainly iron sulfides, magnetite, dolomite, Ca-phosphate, and ilmenite. Fig. S8 shows TEM images of an MgO-rich olivine crystal (Mg#~100) found at the surface of the Ryugu piece. The olivine grain has a nearly euhedral shape with smooth straight crystal surfaces. Most of the boundaries between the olivine crystal and the surrounding phyllosilicate-rich matrix are sharp (fig. S8C) suggesting that those olivine surfaces were not affected by aqueous alteration. We observe however a small part of the olivine surface is not sharp and mixed with phyllosilicate matrix (fig. S8D). This feature may correspond to surface alteration by aqueous fluid. The presence of olivine grain with minor alteration to phyllosilicate indicates that the olivine grains accreted onto the Ryugu parent body prior to aqueous alteration, which took place ~5 Myr after solar system formation (*3*). These observations further indicate that the survived olivine grains in Ryugu experienced very minor alteration to phyllosilicates.

On an oxygen three-isotope diagram, $\delta^{17}O$ *vs.* $\delta^{18}O$, the compositions of primary minerals in Ryugu and Ivuna are distributed along slope-1 line (Fig. 3). Most data plot closer to the primitive chondrule mineral (PCM) line (*13*) rather than to the carbonaceous chondrite anhydrous mineral (CCAM) line (*11*). The $\Delta^{17}O$ values range from ~ −24‰ to ~ −2‰ for Ryugu, and from ~ −24‰ to ~ 0‰ for Ivuna. Among the Ryugu monomineralic grains, the $\Delta^{17}O$ values of olivine show a bimodal distribution (Fig. 1H): 3 grains are ^{16}O-poor ($\Delta^{17}O$ ~ −5‰) and 3 are ^{16}O-rich ($\Delta^{17}O$ ~ −23‰). Both ^{16}O-poor and ^{16}O-rich grains coexist in the same clasts (Fig. 2). The low-Ca pyroxene is ^{16}O-poor ($\Delta^{17}O$ ~ −4‰). The Mg-Al spinel is ^{16}O-rich ($\Delta^{17}O$ ~ −23‰), whereas the Cr-spinel is ^{16}O-poor ($\Delta^{17}O$ ~ −2‰). The bimodal distribution of $\Delta^{17}O$ is also observed among the Ivuna olivine grains (Fig. 1I): 21 grains are ^{16}O-poor ($\Delta^{17}O$ ~ −7‰ to ~ 0‰) and 7 are ^{16}O-rich ($\Delta^{17}O$ ~ −23‰). The two low-Ca pyroxene grains measured in Ivuna are ^{16}O-poor ($\Delta^{17}O$ ~ −5‰). The Mg-Al spinel is ^{16}O-rich ($\Delta^{17}O$ ~ −23‰). The ^{16}O-rich olivine grains in Ryugu and Ivuna have Mg# > 97 whereas the ^{16}O-poor olivine grains show much larger range of Mg#, from ~57 to ~99 (fig. S10).

A sub-rounded AOA, composed of nearly pure forsterite (Mg#~99), diopside, anorthite, and tiny Mg-Al spinel grains was also found in Ivuna (Fig. 4, A and C). This is the first discovery of an AOA in CI chondrites. The texture and mineralogy of the AOA is like those in primitive carbonaceous chondrites (*10*). We also found an inclusion composed of forsteritic olivine (Mg# > 98), Mg-Al spinel, and interstitial phyllosilicates in Ivuna (Fig. 4, B and D). The texture and mineralogy of this inclusion resemble AOAs enclosing small spinel-anorthite±melilite-diopside-bearing CAIs (*10*) which experienced extensive aqueous alteration resulting in replacement of CAI anhydrous silicates by phyllosilicates. The O isotopic compositions of the Ivuna AOA and spinel-olivine inclusion plot along ~slope-1 line and have nearly identical $\Delta^{17}O$, −23.6 ± 0.3‰ (2σ, n = 5) and −24.0 ± 1.7‰ (n = 3), respectively (Fig. 4, E and F).

Discussion

Bimodal distributions of O isotopic compositions of primary minerals

The bimodal distribution of $\Delta^{17}O$ for the Ivuna olivines determined here based on *in situ* analyses on a polished section and the peak $\Delta^{17}O$ value of ~ −6‰ among ^{16}O-poor olivines (Fig. 1I) contrast with previously reported data for olivine grains (> 50 μm, n = 19) isolated from the CI chondrites Orgueil and Ivuna (*4, 6*), where only ^{16}O-poor olivines ($\Delta^{17}O$ range from ~ −6‰ to +3‰ with a peak value of ~0‰) were observed (Fig. 1E). The observed differences between these datasets may reflect a sample bias. Comprehensive mineralogical studies of olivine grains in CI chondrites Alais, Orgueil and Ivuna show that most of olivine grains are < 30 μm in size (*5, 18, 19*). Similarly, all olivine grains observed in the polished sample of Ivuna in this study are < 30 μm. 79% of olivines in this study have Mg# > 97 (fig. S9B), while 77% of olivines by (*5, 18, 19*) have Mg# > 97 (n = 69) (fig. S9C). These consistencies of size and chemical distribution indicate that our dataset of olivine grains from Ivuna is representative of CI chondrites. In contrast, the CI olivine grains measured for O isotopic compositions previously were hand-picked from disaggregated meteorites, were larger than 50 μm, and had predominantly Mg# < 97 (Fig. 1E and fig. S9D) (*4, 6*). Therefore, literature data (*4, 6*) may have been biased sampling and are probably not representative distribution for CI chondrites. A recent study (*7*) also found both ^{16}O-poor and ^{16}O-rich olivines from the CI chondrites Ivuna and Alais by *in situ* O-isotope analysis of those grains embedded in the matrices (Fig. 1F).

Liu et al. [*9*] argued that O isotopic exchange might have occurred in olivine grains in Ryugu. Similarly, Mg-Fe exchange during aqueous alteration (*3*) might have caused an Fe-enrichment in the grains. Such exchanges are however unlikely due to the slow volume diffusivity of cations and oxygen in olivine at the temperature relevant to aqueous alteration in Ryugu. Using the Mg-Fe interdiffusion coefficient for olivine (*20*), Mg-Fe exchange at a temperature of ~300°C, that is a much higher temperature than the inferred maximum temperatures of aqueous alteration on the CI parent body and Ryugu (< ~150°C) (*2, 4, 21*), is calculated to occur in 1 μm scale in olivine for 10^{10} years. The time scale is unreasonably long for the aqueous alteration. Moreover, some olivine grains in Ryugu and Ivuna are chemically zoned but this cannot be explained by diffusion. The Mg-Fe chemical zonings are often observed in olivine grains in ferroan porphyritic (type II) chondrules in primitive carbonaceous chondrites (*13, 14, 22*). The micro-scale heterogeneity of Mg-Fe distributions in olivine grains (fig. S6, F and G) indicates the diffusion distance of Mg-Fe in olivine was less than 1 μm scale. Therefore, effect of the Mg-Fe exchange is negligible in olivine. Oxygen self-diffusion rates are much smaller than the Mg-Fe interdiffusion rates in olivine for all temperatures (*23*). Oxygen isotopic exchange is, therefore, also excluded in olivine. Similarly, effects of diffusive exchanges of Mg-Fe and O-isotopes in pyroxene and spinel by solid-state diffusion are negligible at the temperatures experienced by the CI parent body and Ryugu (*24–27*). Therefore, the chemical and O isotopic compositions of olivine, low-Ca pyroxene, and spinel in Ryugu and Ivuna have not been disturbed after accretion, and they most likely preserve pre-accretion signatures acquired in the solar nebula environment.

Olivine grains in Ryugu show a bimodal distribution of $\Delta^{17}O$, ~ −23‰ and ~ −5‰ (Fig. 1H), similar to that observed for olivine grains in Ivuna (Fig. 1I). The O isotopic compositions of low-Ca pyroxene and Mg-Al spinel in Ryugu are also similar to those measured in Ivuna minerals (Fig. 3). We conclude that primary minerals in Ryugu and CI chondrites have similar characteristics and sampled two isotopically distinct materials, ^{16}O-rich and ^{16}O-poor.

Origin of ^{16}O-poor primary minerals in Ryugu and Ivuna

The ^{16}O-poor olivine and low-Ca pyroxene in Ryugu and Ivuna have $\Delta^{17}O$ values ranging from ~ −7‰ to ~ 0‰ (Fig. 1, H and I). This range is consistent with those observed for olivine and low-Ca pyroxene in porphyritic chondrules from several carbonaceous chondrite groups [CV

(Vigarano-type), CM (Mighei-type), CO (Ornans-type)] and the ungrouped carbonaceous chondrite Acfer 094 (Fig. 1, A to D). The Ivuna olivine grains with Mg# < 97 have typically higher $\Delta^{17}O$ (> ~ −2‰) than more Mg-rich olivine (~ −6‰) (Fig. 1I and fig. S10). Such relationships between $\Delta^{17}O$ and Mg# are often observed for olivine (Fig. 1, A to D) and low-Ca pyroxene phenocrysts in chondrules from carbonaceous chondrites (*13–17*). Moreover, the most frequent $\Delta^{17}O$ value (~ −6‰) for the Ivuna olivine is identical to those for chondrules (Fig. 1, A to D and I). The chemical features of the Ryugu and Ivuna olivine grains are consistent with those observed for olivine in chondrules of the primitive carbonaceous chondrites (fig. S11). Fe,Ni-metal blebs in forsteritic grain seen in the Ivuna sample (fig. S7A) are frequently observed in Mg-rich porphyritic chondrules from carbonaceous chondrites (*13–17*). The Ryugu Cr-spinel has $\Delta^{17}O$ value of −1.8 ± 1.4‰. Chrome-spinel is commonly observed in type II chondrules in carbonaceous chondrites (*28*). The majority of type II chondrules in carbonaceous chondrites have $\Delta^{17}O$ ~ −2‰ (*13–17*). Therefore, we infer that the Ryugu Cr-spinel most likely originated from a carbonaceous chondrite type II chondrule-like melt. Like CIs, Ryugu is devoid of chondrules, but the ^{16}O-poor olivine, low-Ca pyroxene, and Cr-spinel grains in Ryugu and Ivuna most likely represent fragments of chondrule-like objects.

Origin of ^{16}O-rich primary minerals in Ryugu and Ivuna

The AOA and spinel-olivine inclusion found in Ivuna (Fig. 4) are textually, mineralogically, and isotopically like AOAs and spinel-rich, fine-grained CAIs in carbonaceous chondrites (*10, 29–33*). These objects most likely formed by condensation from an ^{16}O-rich gaseous reservoir. The presence of interstitial phyllosilicates in the spinel-olivine inclusion suggests it subsequently experienced aqueous alteration, probably on the Ivuna parent body. The ^{16}O-rich isolated olivine and Mg-Al spinel grains in Ryugu and Ivuna studied here have $\Delta^{17}O$ values identical to those of the Ivuna AOA-like objects and to those of most CAIs and AOAs from other types of carbonaceous chondrites (*31, 33–35*); they consistently show $\Delta^{17}O$ ~ −23‰ to −24‰. Ryugu ^{16}O-rich olivine grains presented by Nakamura et al. [*8*] also show $\Delta^{17}O$ ~ −23‰ (Fig 1G). In contrast, ^{16}O-rich olivine and low-Ca pyroxene in CI chondrites by Morin et al. [*7*] show variations in $\Delta^{17}O$ ranging from −24‰ to −19‰ (Fig 1F). The variations are clearly larger than their given analytical uncertainties of typically ~0.6‰. Further studies are needed to clarify the origin or reason of variable $\Delta^{17}O$ for ^{16}O-rich minerals.

The ^{16}O-rich isolated olivine grains studied here are all Mg-rich (Mg# > 97) (fig. S10) and their CaO contents are < ~0.15 wt% (fig. S11), consistent with compositions for olivine grains of the Ivuna AOA-like objects and those of AOAs from primitive carbonaceous chondrites (*10, 30, 31*). Irregular shapes of Mg-Al spinel grains in Ryugu and Ivuna (figs. S6D and S7C) are consistent with mineralogical textures of spinel-rich, fine-grained CAIs in carbonaceous chondrites (*29, 31, 32*). These observations indicate that the ^{16}O-rich olivine and Mg-Al spinel grains in Ryugu and Ivuna represent fragments of refractory inclusions, and/or isolated grains condensed in the refractory inclusion-forming region. Moreover, the CAI-like mineral assemblages composed of Mg-Al spinel, perovskite, and ±hibonite were reported in the C0040 and C0002 Ryugu samples (*2*). A fragment of melilite-rich (Type A) CAI was discovered in Ivuna (*36*). Micron-sized ^{16}O-rich ($\Delta^{17}O$ ~ −23‰) corundum grains were reported in acid residues of Orgueil (*37*). The presence of ^{16}O-rich refractory inclusion-like objects and isolated mineral grains in Ryugu and Ivuna indicates that fragments of ^{16}O-rich refractory inclusions were also clearly one of the building blocks of the Ryugu and Ivuna parent body. The presence of both ^{16}O-poor chondrule-like and ^{16}O-rich refractory inclusion-like minerals in Ryugu and Ivuna suggests that some of building blocks of Ryugu and Ivuna are similar to those of other carbonaceous chondrite groups.

Implications for the accretion region of Ryugu and Ivuna parent bodies

The ^{16}O-rich objects in Ryugu and Ivuna, texturally and isotopically similar to refractory inclusions, most likely formed in a high-temperature, innermost region of the solar protoplanetary disk, possibly < ~0.1 au (astronomical units) from the proto-Sun (*38*) where the ambient gas was primarily ^{16}O-rich (*12*). The accretion regions of the Ryugu and CI chondrites parent body are inferred to be beyond 3–4 au (*2*) and possibly as far as ~15 au from the Sun (*39*). Whole rock Fe isotopic compositions of Ryugu and CI chondrites also imply that they are accreted in the outer Solar System (*40*). In this context, the ^{16}O-rich primary minerals were transported outward from the innermost region to the outerskirts of the disk system. The similar conclusion was reached to explain the presence of high-temperature minerals in the comet 81P/Wild2 samples (*41, 42*).

Normal-sized chondrules (~100 to ~2000 μm in apparent diameter) (*43*) that are commonly observed in most groups of carbonaceous chondrites, as well as their pseudomorphs, have not been identified in Ryugu and CI chondrites (*2–9*; this study). This cannot be explained by extensive aqueous alteration experienced by the Ryugu and CI parent bodies, because chondrule pseudomorphs are preserved in the nearly completely aqueously altered CM and CR (Renazzo-type) carbonaceous chondrites (*44, 45*). Furthermore, isotopic fractionations of moderately volatile elements in CIs are consistent with accretion from material largely devoid of chondrules (*46*). The ^{16}O-poor olivine, low-Ca pyroxene, and Cr-spinel in Ryugu and Ivuna are typically < 30 μm in size and most likely represent chondrule fragments. These observations suggest that chondrule-forming events were rare at the accretion time and/or near the accretion region of the Ryugu and CI parent bodies compared to those of other carbonaceous chondrite groups.

The ratios of the refractory inclusion-like ^{16}O-rich olivine grains to the chondrule-like ^{16}O-poor olivine grains studied here are 3:3 for Ryugu and 7:21 for Ivuna, respectively (Fig. 1, H and I). If we combined with the data of Nakamura et al. [*8*] (Fig. 1G), the proportion for Ryugu is 6:7. These proportions are like that for olivine grains of the comet 81P/Wild2 samples of 4:10 (Fig. 1J). On the other hand, the ratios for Ryugu, Ivuna, and comet 81P/Wild2 are in sharp contrast with ratios for other carbonaceous chondrite groups. In the highly hydrated carbonaceous chondrite Tagish Lake (C-ungrouped) which contains rare chondrules (*47*) and that was inferred to have accreted at > 10 au from the Sun (*48*), the ratio for isolated olivine grains, embedded in matrices, is 1:21 (*49*) (Fig. 1K); ^{16}O-rich olivine is much rarer than those for Ryugu, Ivuna, and comet 81P/Wild2. In other carbonaceous chondrites (CO, CV, CM, and C-ungrouped), none of 31 isolated olivine grains exhibit refractory inclusion-like ^{16}O-rich compositions, instead all of them show chondrule-like ^{16}O-poor compositions (*50*). If we estimate the abundance of refractory inclusion-like ^{16}O-rich olivine among all olivine grains, that for Ryugu and Ivuna is 32 ± 14% (2σ). The abundance for other carbonaceous chondrite groups (CO, CV, CM, and C-ungrouped including Tagish Lake) is 2 ± 4%, and that for 81P/Wild2 samples is 29 ± 24%. The abundance of refractory inclusion-like olivine for Ryugu and Ivuna (32 ± 14%) and that for 81P/Wild2 samples (29 ± 24%) are very similar to each other. On the other hand, that for Ryugu and Ivuna (32 ± 14%) is clearly different from that for other carbonaceous chondrite groups (2 ± 4%). Moreover, in CV carbonaceous chondrites, characterized by the highest abundance of refractory inclusions among carbonaceous chondrites, the volume ratio of refractory inclusions to chondrules is 1:10 to 1:5 (*51, 52*).

The ratio for olivine in Ryugu and Ivuna that can be tied to refractory inclusions and chondrules is like what has been documented in comet 81P/Wild2. The relative paucity of chondrule-derived anhydrous grains in Ryugu, Ivuna, and 81P/Wild2 could be due to efficient outward transport of refractory inclusions-derived grains (*37*) formed at the earliest stage of

evolution of the solar protoplanetary disk (*31, 32*) and/or rarer chondrule-formation events near the accretion regions. We infer that the accretion region of Ryugu and CI parent bodies is distinct from those for other carbonaceous chondrite groups including Tagish Lake, and could be closer to the accretion region of 81P/Wild2 comet.

Materials and Methods

Sample preparation

Polished sections of C0002-C1001 (fig. S3) and Ivuna-HK2 (fig. S5) made from the Ryugu sample C0002 and the Ivuna CI chondrite were used for mineralogical and petrological observations and *in situ* O-isotope measurements by secondary ion mass spectrometry (SIMS). The samples were individually embedded in 1-inch epoxy disks using the Buehler EpoxiCure 2 Resin. After embedding, their sample surface sides were also impregnated with the resin in vacuum, to avoid collapsing the fragile samples during polishing. The sample disks were polished with an automatic polishing machine (Musashino Denshi MA-200e) at Hokkaido University. Diamond slurry with polycrystalline diamond particles of ~3 μm dissolved in ethylene glycol sprayed on a copper polishing plate was used to obtain flat surface of the sample disks. During the flattening, the sample surfaces were impregnated with the resin in vacuum a few times. Subsequently, ~1 μm diamond slurry sprayed on a tin-antimony alloy polishing plate and on polishing cloth were used to finalize the polishing. These procedures were adopted to obtain flat and smooth surface for anhydrous minerals, which is critical for the quality of SIMS measurements. Only > 99.5% ethanol was used for cleaning during and after the polishing. The polished sections were coated with a thin (~5 nm) gold film using a Leica EM ACE600 coater at Hokkaido University, for backscattered electron (BSE) and X-ray imaging, and elemental analysis before *in situ* O-isotope measurements.

Electron microscopy

BSE images were obtained using a field-emission type scanning electron microscope (FE-SEM; JEOL JSM-7000F) at Hokkaido University. X-ray elemental analyses were conducted with a 15 keV electron beam using an energy dispersive X-ray spectrometer (EDS; Oxford X-Max 150) installed on the FE-SEM. Beam currents of ~2 nA and ~1 nA were employed for the X-ray mapping and quantitative analysis, respectively. Quantitative calculations were conducted using Oxford AZtec software. We used in-house standards, such as San Carlos olivine and Mn metal, for the standardization. X-ray elemental maps covering the entire polished sections of C0002-C1001 (fig. S3) and Ivuna-HK2 (fig. S5) were obtained with pixel sizes of 0.24 μm and 0.48 μm, respectively, to systematically find out olivine, pyroxene, and spinel grains that can be measured for O isotopic compositions with SIMS. Representative chemical compositions of the primary minerals are shown in table S1. After electron microscopy was completed, the polished sections were recoated with an additional thin (~65 nm) gold film for SIMS measurements.

For the transmission electron microscopy (TEM) of olivine in Ryugu, we used a fine grain (A104-009008) from the first touchdown site. We observed the grain using FE-SEM (JEOL JSM-7001F) at Kyoto University. Then, electron-transparent sections were extracted from the region of interest on the Ryugu piece using a focused ion beam (FIB) system (Helios NanoLab G3 CX at Kyoto University). The Ryugu piece was coated with an electron-beam-deposited Pt layer (at 2 kV) followed by a Ga ion-beam-deposited Pt layer (at 30 kV). The sections of a few tens of micrometers in size were extracted and were thinned to 50 to 200 nm using 16–30 keV Ga^+ beam and finally cleaned using 2 keV Ga^+ beam at 77 pA. The FIB sections were analyzed using an FE-TEM (JEOL JEM 2100F) equipped with an EDS (JEOL JED-2300T) at Kyoto University. Bright-field TEM

images, selected-area electron-diffraction (SAED) patterns, scanning transmission electron microscopy (STEM) images at 200 kV were obtained using a CCD or CMOS camera (Gatan Orius200D, Rio9). EDS analysis was performed in STEM mode. Quantitative elemental abundances were calculated using ζ-factor method (*53*).

In situ O-isotope measurements by secondary ion mass spectrometry (SIMS)

The O isotopic compositions of olivine, pyroxene, and spinel in Ryugu and Ivuna were measured *in situ* with the Cameca ims-1280HR SIMS instrument at Hokkaido University. The analytical and instrumental settings were established by Kawasaki et al. [*35*]. The polished sections were coated with a thin (~70 nm) gold film. Measurement spots are shown in fig. S12 to S51. A $^{133}Cs^{+}$ primary beam accelerated to 20 keV was employed in the experiment. A normal-incidence electron flood gun was used for electrostatic charge compensation of the analyzing areas during the measurements. Negative secondary ions ($^{16}O^{-}$, $^{17}O^{-}$, and $^{18}O^{-}$) were measured simultaneously in the multicollection mode. The mass resolution of $M/\Delta M$ for $^{17}O^{-}$ was set at >6000 to resolve $^{17}O^{-}$ from $^{16}OH^{-}$, while that for $^{16}O^{-}$ and $^{18}O^{-}$ was ~2000. The automatic centering program (DTFA and magnetic field) was applied before data collection.

Analyzed areas were precisely determined according to scanning ion image of $^{16}O^{-}$ collected by a multicollector electron multiplier (EM; designated as L2) which was not used for the data collection. Before measurements, we made a few sputtered craters near measurement targets using 10–30 pA primary beam by the SIMS and then electron images were obtained by the FE-SEM to obtain distances from the sputtered craters to the measurement targets. The craters were visible in $^{16}O^{-}$ scanning images and used to locate the target minerals.

The reported uncertainties in the O-isotopic compositions were the larger of the external reproducibility of standard measurements (2 standard deviation, 2SD) or internal precision (2 standard error of cycle data) of samples. Measurement spots were observed by the FE-SEM after SIMS measurements. The data from spots with inclusions and overlapping matrix minerals were rejected. The reasons of all the rejected spots are written in fig. S12 to S51 and data S1.

We used three conditions with different primary beam currents depending on mineral sizes. An ~1 nA primary beam with elliptical shape of 6 × 8 μm was used for the measurement of olivine grains in Ivuna. The primary beam was rastered over an 8 × 8 μm^2 area during the presputtering for 60 seconds and then the raster size was reduced to 1 × 1 μm^2 for the data collection. $^{16}O^{-}$, $^{17}O^{-}$, and $^{18}O^{-}$ were measured using a multicollector Faraday cup (FC; 10^{10} Ω, designated as L'2), an axial FC (10^{12} Ω), and a multicollector FC (10^{12} Ω, designated as H1), respectively. The secondary ion intensity of $^{16}O^{-}$ was ~1.5–1.7 × 10^{9} cps. The data were collected for 30 cycles with 4 seconds integration time per cycle. Obtained count rates were corrected for FC background, monitored during the presputtering of every measurement, and relative yield of each detector. The $^{16}OH^{-}$ count rate was measured immediately after the measurements and we made a small tail correction on $^{17}O^{-}$, although its contribution to $^{17}O^{-}$ was smaller than ~0.1‰. Typical uncertainties for $\delta^{17}O$, $\delta^{18}O$, and $\Delta^{17}O$ were 0.6‰, 0.3‰, and 0.6‰ (2σ), respectively.

An ~30 pA primary beam with elliptical shape of ~2 × 3 μm (~2.5 × 3.5 μm including beam halo) was used for the measurement of olivine, pyroxene, and Cr-spinel in Ryugu and Ivuna. $^{16}O^{-}$, $^{17}O^{-}$, and $^{18}O^{-}$ were measured using a multicollector FC (10^{11} Ω, designated as L1), an axial EM, and a multicollector EM (designated as H2), respectively. The secondary ion intensities of $^{16}O^{-}$ were ~1.7–2.9 × 10^{7} cps, ~2.2 × 10^{7} cps, and ~2.9 × 10^{7} cps for olivine, pyroxene, and Cr-spinel, respectively. The data were collected for 60 cycles with 4 seconds integration time per cycle. Obtained count rates were corrected for FC background, EM dead time, and relative yield of each detector. Typical uncertainties for $\delta^{17}O$, $\delta^{18}O$, and $\Delta^{17}O$ were 1.6‰, 1.0‰, and 1.7‰, respectively.

An ~3 pA primary beam with elliptical shape of 0.8 × 1.3 μm (~1.0 × 2.0 μm including beam halo) was used for the measurement of olivine, pyroxene, and Mg-Al spinel in Ryugu and Ivuna. Detector settings are the same with those for the ~30 pA condition above. The secondary ion intensities of $^{16}O^-$ were ~1.5–2.1 × 10^6 cps. The data were collected for 200 cycles with 4 seconds integration time per cycle. The $^{16}OH^-$ count rate was measured immediately after the measurements, but we did not make a tail correction on $^{17}O^-$ because its contribution to $^{17}O^-$ was calculated as typically ~0.03‰ and up to ~0.2‰, comparable to that for standards. Typical uncertainties for $\delta^{17}O$, $\delta^{18}O$, and $\Delta^{17}O$ were 3.1‰, 2.0‰, and 3.1‰, respectively.

San Carlos olivine (Mg# = 89; $\delta^{18}O$ = 5.2‰), synthetic enstatite ($\delta^{18}O$ = 10.55‰), and Russian spinel ($\delta^{18}O$ = 8.5‰) (*54*) were used as standards to correct the instrumental mass fractionation for olivine, pyroxene, and spinel, respectively. Since Mg# of olivine grains are larger than 76, except for an olivine grain in Ivuna with Mg#~57, variations in instrumental mass fractionation correlated with Mg# of olivine from that of San Carlos olivine (*55*) could be insignificant in the analytical uncertainties of this study.

References

1. S. Tachibana, H. Sawada, R. Okazaki, Y. Takano, K. Sakamoto, Y. N. Miura, C. Okamoto, H. Yano, S. Yamanouchi, P. Michel, Y. Zhang, S. Schwartz, F. Thuillet, H. Yurimoto, T. Nakamura, T. Noguchi, H. Yabuta, H. Naraoka, A. Tsuchiyama, N. Imae, K. Kurosawa, A. M. Nakamura, K. Ogawa, S. Sugita, T. Morota, R. Honda, S. Kameda, E. Tatsumi, Y. Cho, K. Yoshioka, Y. Yokota, M. Hayakawa, M. Matsuoka, N. Sakatani, M. Yamada, T. Kouyama, H. Suzuki, C. Honda, T. Yoshimitsu, T. Kubota, H. Demura, T. Yada, M. Nishimura, K. Yogata, A. Nakato, M. Yoshitake, A. I. Suzuki, S. Furuya, K. Hatakeda, A. Miyazaki, K. Kumagai, T. Okada, M. Abe, T. Usui, T. R. Ireland, M. Fujimoto, T. Yamada, M. Arakawa, H. C. Connolly Jr, A. Fujii, S. Hasegawa, N. Hirata, C. Hirose, S. Hosoda, Y. Iijima, H. Ikeda, M. Ishiguro, Y. Ishihara, T. Iwata, S. Kikuchi, K. Kitazato, D. S. Lauretta, G. Libourel, B. Marty, K. Matsumoto, T. Michikami, Y. Mimasu, A. Miura, O. Mori, K. Nakamura-Messenger, N. Namiki, A. N. Nguyen, L. R. Nittler, H. Noda, R. Noguchi, N. Ogawa, G. Ono, M. Ozaki, H. Senshu, T. Shimada, Y. Shimaki, K. Shirai, S. Soldini, T. Takahashi, Y. Takei, H. Takeuchi, R. Tsukizaki, K. Wada, Y. Yamamoto, K. Yoshikawa, K. Yumoto, M. E. Zolensky, S. Nakazawa, F. Terui, S. Tanaka, T. Saiki, M. Yoshikawa, S. Watanabe, Y. Tsuda, Pebbles and sand on asteroid (162173) Ryugu: In situ observation and particles returned to Earth. *Science* **375**, 1011–1016 (2022).
2. T. Nakamura, M. Matsumoto, K. Amano, Y. Enokido, M. E. Zolensky, T. Mikouchi, H. Genda, S. Tanaka, M. Y. Zolotov, K. Kurosawa, S. Wakita, R. Hyodo, H. Nagano, D. Nakashima, Y. Takahashi, Y. Fujioka, M. Kikuiri, E. Kagawa, M. Matsuoka, A. J. Brearley, A. Tsuchiyama, M. Uesugi, J. Matsuno, Y. Kimura, M. Sato, R. E. Milliken, E. Tatsumi, S. Sugita, T. Hiroi, K. Kitazato, D. Brownlee, D. J. Joswiak, M. Takahashi, K. Ninomiya, T. Takahashi, T. Osawa, K. Terada, F. E. Brenker, B. J. Tkalcec, L. Vincze, R. Brunetto, A. Aléon-Toppani, Q. H. S. Chan, M. Roskosz, J.-C. Viennet, P. Beck, E. E. Alp, T. Michikami, Y. Nagaashi, T. Tsuji, Y. Ino, J. Martinez, J. Han, A. Dolocan, R. J. Bodnar, M. Tanaka, H. Yoshida, K. Sugiyama, A. J. King, K. Fukushi, H. Suga, S. Yamashita, T. Kawai, K. Inoue, A. Nakato, T. Noguchi, F. Vilas, A. R. Hendrix, C. Jaramillo-Correa, D. L. Domingue, G. Dominguez, Z. Gainsforth, C. Engrand, J. Duprat, S. S. Russell, E. Bonato, C. Ma, T. Kawamoto, T. Wada, S. Watanabe, R. Endo, S. Enju, L. Riu, S. Rubino, P. Tack, S. Takeshita, Y. Takeichi, A. Takeuchi, A. Takigawa, D. Takir, T. Tanigaki, A. Taniguchi, K. Tsukamoto, T. Yagi, S. Yamada, K. Yamamoto, Y. Yamashita, M. Yasutake, K. Uesugi, I. Umegaki, I. Chiu, T. Ishizaki, S. Okumura, E. Palomba, C. Pilorget, S. M. Potin, A. Alasli, S. Anada, Y. Araki, N. Sakatani, C. Schultz, O. Sekizawa, S. D. Sitzman, K. Sugiura, M. Sun, E. Dartois, E. De Pauw, Z. Dionnet, Z. Djouadi, G. Falkenberg, R. Fujita, T. Fukuma, I. R. Gearba, K. Hagiya, M. Y. Hu, T. Kato, T. Kawamura, M. Kimura, M. K. Kubo,

F. Langenhorst, C. Lantz, B. Lavina, M. Lindner, J. Zhao, B. Vekemans, D. Baklouti, B. Bazi, F. Borondics, S. Nagasawa, G. Nishiyama, K. Nitta, J. Mathurin, T. Matsumoto, I. Mitsukawa, H. Miura, A. Miyake, Y. Miyake, H. Yurimoto, R. Okazaki, H. Yabuta, H. Naraoka, K. Sakamoto, S. Tachibana, H. C. ConnollyJr., D. S. Lauretta, M. Yoshitake, M. Yoshikawa, K. Yoshikawa, K. Yoshihara, Y. Yokota, K. Yogata, H. Yano, Y. Yamamoto, D. Yamamoto, M. Yamada, T. Yamada, T. Yada, K. Wada, T. Usui, R. Tsukizaki, F. Terui, H. Takeuchi, Y. Takei, A. Iwamae, H. Soejima, K. Shirai, Y. Shimaki, H. Senshu, H. Sawada, T. Saiki, M. Ozaki, G. Ono, T. Okada, N. Ogawa, K. Ogawa, R. Noguchi, H. Noda, M. Nishimura, N. Namiki, S. Nakazawa, T. Morota, A. Miyazaki, A. Miura, Y. Mimasu, K. Matsumoto, K. Kumagai, T. Kouyama, S. Kikuchi, K. Kawahara, S. Kameda, T. Iwata, Y. Ishihara, M. Ishiguro, H. Ikeda, S. Hosoda, R. Honda, C. Honda, Y. Hitomi, N. Hirata, N. Hirata, T. Hayashi, M. Hayakawa, K. Hatakeda, S. Furuya, R. Fukai, A. Fujii, Y. Cho, M. Arakawa, M. Abe, S. Watanabe, Y. Tsuda, Formation and evolution of Cb-type asteroid Ryugu: Direct evidence from returned samples. *Science* in press. 10.1126/science.abn8671.

3. T. Yokoyama, K. Nagashima, I. Nakai, E. D. Young, Y. Abe, J. Aléon, C. M. O. Alexander, S. Amari, Y. Amelin, K. I. Bajo, M. Bizzarro, A. Bouvier, R. W. Carlson, M. Chaussidon, B.-G. Choi, N. Dauphas, A. M. Davis, T. Di Rocco, W. Fujiya, R. Fukai, I. Gautam, M. K. Haba, Y. Hibiya, H. Hidaka, H. Homma, P. Hoppe, G. R. Huss, K. Ichida, T. Iizuka, T. R. Ireland, A. Ishikawa, M. Ito, S. Itoh, N. Kawasaki, N. T. Kita, K. Kitajima, T. Kleine, S. Komatani, A. N. Krot, M.-C. Liu, Y. Masuda, K. D. McKeegan, M. Morita, K. Motomura, F. Moynier, A. Nguyen, L. Nittler, M. Onose, A. Pack, C. Park, L. Piani, L. Qin, S. S. Russell, N. Sakamoto, M. Schönbächler, L. Tafla, H. Tang, K. Terada, Y. Terada, T. Usui, S. Wada, M. Wadhwa, R. J. Walker, K. Yamashita, Q.-Z. Yin, S. Yoneda, H. Yui, A.-C. Zhang, H. C. ConnollyJr., D. S. Lauretta, T. Nakamura, H. Naraoka, T. Noguchi, R. Okazaki, K. Sakamoto, H. Yabuta, M. Abe, M. Arakawa, A. Fujii, M. Hayakawa, N. Hirata, N. Hirata, R. Honda, C. Honda, S. Hosoda, Y. I. Iijima, H. Ikeda, M. Ishiguro, Y. Ishihara, T. Iwata, K. Kawahara, S. Kikuchi, K. Kitazato, K. Matsumoto, M. Matsuoka, T. Michikami, Y. Mimasu, A. Miura, T. Morota, S. Nakazawa, N. Namiki, H. Noda, R. Noguchi, N. Ogawa, K. Ogawa, T. Okada, C. Okamoto, G. Ono, M. Ozaki, T. Saiki, N. Sakatani, H. Sawada, H. Senshu, Y. Shimaki, K. Shirai, S. Sugita, Y. Takei, H. Takeuchi, S. Tanaka, E. Tatsumi, F. Terui, Y. Tsuda, R. Tsukizaki, K. Wada, S. I. Watanabe, M. Yamada, T. Yamada, Y. Yamamoto, H. Yano, Y. Yokota, K. Yoshihara, M. Yoshikawa, K. Yoshikawa, S. Furuya, K. Hatakeda, T. Hayashi, Y. Hitomi, K. Kumagai, A. Miyazaki, A. Nakato, M. Nishimura, H. Soejima, A. Suzuki, T. Yada, D. Yamamoto, K. Yogata, M. Yoshitake, S. Tachibana, H. Yurimoto, Samples returned from the asteroid Ryugu are similar to Ivuna-type carbonaceous meteorites. *Science* in press. 10.1126/science.abn7850.
4. L. A. Leshin, A. E. Rubin, K. D. McKeegan, The oxygen isotopic composition of olivine and pyroxene from CI chondrites. *Geochim. Cosmochim. Acta* **61**, 835–845 (1997).
5. J. Alfing, M. Patzek, A. Bischoff, Modal abundances of coarse-grained (>5 μm) components within CI-chondrites and their individual clasts – Mixing of various lithologies on the CI parent body(ies). *Geochemistry* **79**, 125532 (2019).
6. M. Piralla, Y. Marrocchi, M. J. Verdier-Paoletti, L. G. Vacher, J. Villeneuve, L. Piani, D. V. Bekaert, M. Gounelle, Primordial water and dust of the Solar System: Insights from in situ oxygen measurements of CI chondrites. *Geochim. Cosmochim. Acta* **269**, 451–464 (2020).
7. G. L. F. Morin, Y. Marrocchi, J. Villeneuve, E. Jacquet, ^{16}O-rich anhydrous silicates in CI chondrites: Implications for the nature and dynamics of dust in the solar accretion disk. *Geochim. Cosmochim. Acta* in press. 10.1016/j.gca.2022.06.017.
8. E. Nakamura, K. Kobayashi, R. Tanaka, T. Kunihiro, H. Kitagawa, C. Potiszil, T. Ota, C. Sakaguchi, M. Yamanaka, D. M. Ratnayake, H. Tripathi, R. Kumar, M. L. Avramescu, H. Tsuchida, Y. Yachi, H. Miura, M. Abe, R. Fukai, S. Furuya, K. Hatakeda, T. Hayashi, Y. Hitomi, K. Kumagai, A. Miyazaki, A. Nakato, M. Nishimura, T. Okada, H. Soejima, S. Sugita, A. Suzuki,

T. Usui, T. Yada, D. Yamamoto, K. Yogata, M. Yoshitake, M. Arakawa, A. Fujii, M. Hayakawa, N. Hirata, N. Hirata, R. Honda, C. Honda, S. Hosoda, Y. I. Iijima, H. Ikeda, M. Ishiguro, Y. Ishihara, T. Iwata, K. Kawahara, S. Kikuchi, K. Kitazato, K. Matsumoto, M. Matsuoka, T. Michikami, Y. Mimasu, A. Miura, T. Morota, S. Nakazawa, N. Namiki, H. Noda, R. Noguchi, N. Ogawa, K. Ogawa, C. Okamoto, G. Ono, M. Ozaki, T. Saiki, N. Sakatani, H. Sawada, H. Senshu, Y. Shimaki, K. Shirai, Y. Takei, H. Takeuchi, S. Tanaka, E. Tatsumi, F. Terui, R. Tsukizaki, K. Wada, M. Yamada, T. Yamada, Y. Yamamoto, H. Yano, Y. Yokota, K. Yoshihara, M. Yoshikawa, K. Yoshikawa, M. Fujimoto, S. I. Watanabe, Y. Tsuda, On the origin and evolution of the asteroid Ryugu: A comprehensive geochemical perspective, *Proc. Jpn. Acad., Ser. B*, 98(6), 227–282.

9. M.-C. Liu, K. A. McCain, N. Matsuda, A. Yamaguchi, M. Kimura, N. Tomioka, M. Ito, M. Uesugi, N. Imae, N. Shirai, T. Ohigashi, R. C. Greenwood, K. Uesugi, A. Nakato, K. Yogata, H. Yuzawa, Y. Kodama, K. Hirahara, I. Sakurai, I. Okada, Y. Karouji, S. Nakazawa, T. Okada, T. Saiki, S. Tanaka, F. Terui, M. Yoshikawa, A. Miyazaki, M. Nishimura, T. Yada, M. Abe, T. Usui, S.-i. Watanabe, Y. Tsuda, In-situ oxygen isotope study of anhydrous minerals in a Ryugu particle: Implications for the precursors to CI-chondrite parent bodies. *proceedings of the 53rd Lunar and Planetary Science Conference,* Abstract #2276 (2022).
10. A. N. Krot, M. I. Petaev, S. S. Russell, S. Itoh, T. J. Fagan, H. Yurimoto, L. Chizmadia, M. K. Weisberg, M. Komatsu, A. A. Ulyanov, K. Keil, Amoeboid olivine aggregates and related objects in carbonaceous chondrites: records of nebular and asteroid processes. *Geochemistry* **64**, 185–239 (2004).
11. R. N. Clayton, N. Onuma, L. Grossman, T. K. Mayeda, Distribution of the presolar component in Allende and other carbonaceous chondrites. *Earth Planet. Sci. Lett.* **34**, 209–224 (1977).
12. H. Yurimoto, A. N. Krot, B. G. Choi, J. Aleon, T. Kunihiro, A. J. Brearley, Oxygen isotopes in chondritic components. *Rev. Mineral. Geochem.* 141–186 (2008).
13. T. Ushikubo, M. Kimura, N. T. Kita, J. W. Valley, Primordial oxygen isotope reservoirs of the solar nebula recorded in chondrules in Acfer 094 carbonaceous chondrite. *Geochim. Cosmochim. Acta* **90**, 242–264 (2012).
14. T. J. Tenner, T. Ushikubo, E. Kurahashi, N. T. Kita, H. Nagahara, Oxygen isotope systematics of chondrule phenocrysts from the CO3.0 chondrite Yamato 81020: Evidence for two distinct oxygen isotope reservoirs. *Geochim. Cosmochim. Acta* **102**, 226–245 (2013).
15. N. Chaumard, C. Defouilloy, N. T. Kita, Oxygen isotope systematics of chondrules in the Murchison CM2 chondrite and implications for the CO-CM relationship. *Geochim Cosmochim Acta* **228**, 220–242 (2018).
16. A. T. Hertwig, C. Defouilloy, N. T. Kita, Formation of chondrules in a moderately high dust enriched disk: evidence from oxygen isotopes of chondrules from the Kaba CV3 chondrite. *Geochim Cosmochim Acta* **224**, 116–131 (2018).
17. T. J. Tenner, T. Ushikubo, D. Nakashima, D. L. Schrader, M. K. Weisberg, M. Kimura, N. T. Kita, "Oxygen Isotope Characteristics of Chondrules from Recent Studies by Secondary Ion Mass Spectrometry" in *Chondrules,* S. S. Russell, H. C. Connolly Jr., A. N. Krot. Eds. (Cambridge University Press, 2018), pp. 196–246.
18. I. M. Steele, Minor elements in forsterites of Orgueil (C1), Alais (C1) and two interplanetary dust particles compared to C2-C3-UOC forsterites. *Meteoritics* **25**, 301–307 (1990).
19. D. R. Frank, M. E. Zolensky, L. Le, Olivine in terminal particles of Stardust aerogel tracks and analogous grains in chondrite matrix. *Geochim. Cosmochim. Acta* **142**, 240–259 (2014).
20. R. Dohmen, H.-W. Becker, S. Chakraborty, Fe–Mg diffusion in olivine I: experimental determination between 700 and 1,200°C as a function of composition, crystal orientation and oxygen fugacity. *Phys. Chem. Miner.* **34**, 389–407 (2007).
21. R. N. Clayton, T. K. Mayeda, Oxygen isotope studies of carbonaceous chondrites. *Geochim. Cosmochim. Acta* **63**, 2089–2104 (1999).

22. H. Yurimoto, J. Wasson, Extremely rapid cooling of a carbonaceous-chondrite chondrule containing very ^{16}O-rich olivine and a ^{26}Mg-excess. *Geochim. Cosmochim. Acta* **66**, 4355–4363 (2002).
23. Y. Oishi, K. Ando, "Oxygen self-diffusion coefficent in single-crystal forsterite" in *Phys. Earth Planet. Inter.*, I. Sunagawa, Ed. (Terra Science Publishing Company, 1984), pp. 271–280.
24. K. Muehlenbachs, I. Kushiro, Oxygen isotopic exchange and equilibrium of silicates with CO_2 and O_2. *Carnegie Inst. Wash. Year B.* **73**, 232–236 (1974).
25. F. J. Ryerson, K. D. McKeegan, Determination of oxygen self-diffusion in åkermanite, anorthite, diopside, and spinel: Implications for oxygen isotopic anomalies and the thermal histories of Ca-Al-rich inclusions. *Geochim. Cosmochim. Acta* **58**, 3713–3734 (1994).
26. H-P. Liermann, J. Ganguly, Diffusion kinetics of Fe^{2+} and Mg in aluminous spinel: Experimental determination and applications. *Geochim. Cosmochim. Acta* **66**, 2903–2913 (2002).
27. T. Müller, R. Dohmen, H. W. Becker, J. H. ter Heege, S. Chakraborty, Fe–Mg interdiffusion rates in clinopyroxene: experimental data and implications for Fe–Mg exchange geothermometers. *Contrib. to Mineral. Petrol.* **166**, 1563–1576 (2013).
28. C. A. Johnson, M. Prinz, Chromite and olivine in type II chondrules in carbonaceous and ordinary chondrites: Implications for thermal histories and group differences. *Geochim. Cosmochim. Acta* **55**, 893–904 (1991).
29. A. N. Krot, G. J. MacPherson, A. A. Ulyanov, M. I. Petaev, Fine-grained, spinel-rich inclusions from the reduced CV chondrites Efremovka and Leoville: I. Mineralogy, petrology, and bulk chemistry. *Meteorit. Planet. Sci.* **39**, 1517–1553 (2004).
30. M. Komatsu, T. J. Fagan, T. Mikouchi, M. I. Petaev, M. E. Zolensky, LIME silicates in amoeboid olivine aggregates in carbonaceous chondrites: Indicator of nebular and asteroidal processes. *Meteorit. Planet. Sci.* **50**, 1271–1294 (2015).
31. T. Ushikubo, T. J. Tenner, H. Hiyagon, N. T. Kita, A long duration of the ^{16}O-rich reservoir in the solar nebula, as recorded in fine-grained refractory inclusions from the least metamorphosed carbonaceous chondrites. *Geochim. Cosmochim. Acta* **201**, 103–122 (2017).
32. N. Kawasaki, S. Wada, C. Park, N. Sakamoto, H. Yurimoto, Variations in initial ^{26}Al/^{27}Al ratios among fine-grained Ca-Al-rich inclusions from reduced CV chondrites. *Geochim. Cosmochim. Acta* **279**, 1–15 (2020).
33. K. Fukuda, D. E. Brownlee, D. J. Joswiak, T. J. Tenner, M. Kimura, N. T. Kita, Correlated isotopic and chemical evidence for condensation origins of olivine in comet 81P/Wild 2 and in AOAs from CV and CO chondrites. *Geochim. Cosmochim. Acta* **293**, 544–574 (2021).
34. K. Makide, K. Nagashima, A. N. Krot, G. R. Huss, I. D. Hutcheon, A. Bischoff, Oxygen- and magnesium-isotope compositions of calcium–aluminum-rich inclusions from CR2 carbonaceous chondrites. *Geochim. Cosmochim. Acta* **73**, 5018–5050 (2009).
35. N. Kawasaki, S. B. Simon, L. Grossman, N. Sakamoto, H. Yurimoto, Crystal growth and disequilibrium distribution of oxygen isotopes in an igneous Ca-Al-rich inclusion from the Allende carbonaceous chondrite. *Geochim. Cosmochim. Acta* **221**, 318–341 (2018).
36. D. R. Frank, G. R. Huss, K. Nagashima, M. E. Zolensky, L. Le, Oxygen, magnesium, and aluminum isotopes in the Ivuna CAI: Re-examining high-temperature fractionations in CI chondrites. *proceedings of 80th Annual Meeting of the Meteoritical Society*, Abstract #6355 (2017).
37. K. Makide, K. Nagashima, A. N. Krot, G. R. Huss, F. J. Ciesla, E. Hellebrand, E. Gaidos, L. Yang, Heterogeneous distribution of ^{26}Al at the birth of the solar system. *Astrophys. J. Lett.* **733**, L31–L34 (2011).
38. K. D. McKeegan, M. Chaussidon, F. Robert, Incorporation of short-lived ^{10}Be in a calcium-aluminum-rich inclusion from the Allende meteorite. *Science* **289**, 1334–1337 (2000).
39. S. J. Desch, A. Kalyaan, C. M. O. D. Alexander, The Effect of Jupiter's Formation on the

654 Distribution of Refractory Elements and Inclusions in Meteorites. *Astrophys. J. Suppl. Ser.* **238**,
655 11 (2018).
656 40. T. Hopp, N. Dauphas, Y. Abe, J. Aléon, C. M. O. D. Alexander, S. Amari, Y. Amelin, K.-i. Bajo,
657 M. Bizzarro, A. Bouvier, R. W. Carlson, M. Chaussidon, B.-G. Choi, A. M. Davis, T. Di Rocco,
658 W. Fujiya, R. Fukai, I. Gautam, M. K. Haba, Y. Hibiya, H. Hidaka, H. Homma, P. Hoppe, G. R.
659 Huss, K. Ichida, T. Iizuka, T. R. Ireland, A. Ishikawa, M. Ito, S. Itoh, N. Kawasaki, N. T. Kita,
660 K. Kitajima, T. Kleine, S. Komatani, A. N. Krot, M.-C. Liu, Y. Masuda, K. D. McKeegan, M.
661 Morita, K. Motomura, F. Moynier, I. Nakai, K. Nagashima, D. Nesvorný, A. Nguyen, L. Nittler,
662 M. Onose, A. Pack, C. Park, L. Piani, L. Qin, S. S. Russell, N. Sakamoto, M. Schönbächler, L.
663 Tafla, H. Tang, K. Terada, Y. Terada, T. Usui, S. Wada, M. Wadhwa, R. J. Walker, K. Yamashita,
664 Q.-Z. Yin, T. Yokoyama, S. Yoneda, E. D. Young, H. Yui, A.-C. Zhang, T. Nakamura, H.
665 Naraoka, T. Noguchi, R. Okazaki, K. Sakamoto, H. Yabuta, M. Abe, A. Miyazaki, A. Nakato,
666 M. Nishimura, T. Okada, T. Yada, K. Yogata, S. Nakazawa, T. Saiki, S. Tanaka, F. Terui, Y.
667 Tsuda, S.-i. Watanabe, M. Yoshikawa, S. Tachibana, H. Yurimoto, Ryugu's nucleosynthetic
668 heritage from the outskirts of the Solar System. *Science Advances*, in press.
669 10.1126/sciadv.add8141.
670 41. K. D. McKeegan, J. Aleon, J. Bradley, D. Brownlee, H. Busemann, A. Butterworth, M.
671 Chaussidon, S. Fallon, C. Floss, J. Gilmour, M. Gounelle, G. Graham, Y. Guan, P. R. Heck, P.
672 Hoppe, I. D. Hutcheon, J. Huth, H. Ishii, M. Ito, S. B. Jacobsen, A. Kearsley, L. A. Leshin, M.
673 C. Liu, I. Lyon, K. Marhas, B. Marty, G. Matrajt, A. Meibom, S. Messenger, S. Mostefaoui, S.
674 Mukhopadhyay, K. Nakamura-Messenger, L. Nittler, R. Palma, R. O. Pepin, D. A.
675 Papanastassiou, F. Robert, D. Schlutter, C. J. Snead, F. J. Stadermann, R. Stroud, P. Tsou, A.
676 Westphal, E. D. Young, K. Ziegler, L. Zimmermann, E. Zinner, Isotopic compositions of
677 cometary matter returned by Stardust. *Science* **314**, 1724–1728 (2006).
678 42. T. Nakamura, T. Noguchi, A. Tsuchiyama, T. Ushikubo, N. T. Kita, J. W. Valley, M. E. Zolensky,
679 Y. Kakazu, K. Sakamoto, E. Mashio, K. Uesugi, T. Nakano, Chondrulelike objects in short-
680 period comet 81P/Wild 2. *Science* **321**, 1664–1667 (2008).
681 43. M. K. Weisberg, T. J. McCoy, A. N. Krot, Systematics and evaluation of meteorites
682 classification. In *Meteorites and The Early Solar System II,* eds. D. Lauretta, H. McSween,
683 University of Arizona Press, pp. 19–53 (2006).
684 44. A. E. Rubin, J. M. Trigo-Rodrıguez, H. Huber, J. T. Wasson, Progressive aqueous alteration of
685 CM carbonaceous chondrites. *Geochim. Cosmochim. Acta* **71**, 2761–2782 (2007).
686 45. E. R. Harju, A. E. Rubin, I. Ahn, B.-G. Choi, K. Ziegler, J. T. Wasson, Progressive aqueous
687 alteration of CR carbonaceous chondrites. *Geochim. Cosmochim. Acta* **139**, 267–292 (2014).
688 46. N. X. Nie, X.-Y. Chen, T. Hopp, J. Y. Hu, Z. J. Zhang, F.-Z. Teng, A. Shahar, N. Dauphas,
689 Imprint of chondrule formation on the K and Rb isotopic compositions of carbonaceous
690 meteorites. *Science Advances* **7**, eabl3929 (2021).
691 47. P. G. Brown, A. R. Hildebrand, M. E. Zolensky, M. Grady, R. N. Clayton, T. K. Mayeda, E.
692 Tagliaferri, R. Spalding, N. D. MacRae, E. L. Hoffman, D. W. Mittlefehldt, J. F. Wacker, J. A.
693 Bird, M. D. Campbell, R. Carpenter, H. Gingerich, M. Glatiotis, E. Greiner, M. J. Mazur, P. J.
694 McCausland, H. Plotkin, T. R. Mazur, The fall, recovery, orbit, and composition of the Tagish
695 Lake meteorite: A new type of carbonaceous chondrite. *Science* **290**, 320–325 (2001).
696 48. W. Fujiya, P. Hoppe, T. Ushikubo, K. Fukuda, P. Lindgren, M. R. Lee, M. Koike, K. Shirai, Y.
697 Sano, Migration of D-type asteroids from the outer Solar System inferred from carbonate in
698 meteorites. *Nature Astronomy* **3**, 910–915 (2019).
699 49. T. Ushikubo, M. Kimura, Oxygen-isotope systematics of chondrules and olivine fragments from
700 Tagish Lake C2 chondrite: Implications of chondrule-forming regions in protoplanetary disk.
701 *Geochimica et Cosmochimica Acta* **293**, 328–343 (2021).
702 50. E. Jacquet, M. Piralla, P. Kersaho, Y. Marrocchi, Origin of isolated olivine grains in
703 carbonaceous chondrites. *Meteoritics & Planetary Science* **56**, 13–33 (2021).

51. D. C. Hezel, S. S. Russell, A. J. Ross, A. T. Kearsley, Modal abundances of CAIs: Implications for bulk chondrite element abundances and fractionations. *Meteorit. Planet. Sci.* **43**, 1879–1894 (2008).
52. D. S. Ebel, C. Brunner, K. Konrad, K. Leftwich, I. Erb, M. Lu, H. Rodriguez, E. J. Crapster-Pregont, J. M. Friedrich, M. K. Weisberg, Abundance, major element composition and size of components and matrix in CV, CO and Acfer 094 chondrites. *Geochim. Cosmochim. Acta* **172**, 322–356 (2016).
53. M. Watanabe, D. B. Williams, The quantitative analysis of thin specimens: a review of progress from the Cliff-Lorimer to the new ζ-factor methods. *J. Microsc.* **221**, 89–109 (2006).
54. H. Yurimoto, H. Nagasawa, Y. Mori, O. Matsubaya, Micro-distribution of oxygen isotopes in a refractory inclusion from the Allende meteorite. *Earth Planet. Sci. Lett.* **128**, 47–53 (1994).
55. T. J. Tenner, D. Nakashima, T. Ushikubo, N. T. Kita, M. K. Weisberg, Oxygen isotope ratios of FeO-poor chondrules in CR3 chondrites: Influence of dust enrichment and H_2O during chondrule formation. *Geochim. Cosmochim. Acta* **148**, 228–250 (2015).
56. K. Nakamura-Messenger, L. P. Keller, S. J. Clemett, S. Messenger, M. Ito, Nanometer-scale anatomy of entire Stardust tracks. *Meteorit. Planet. Sci.* **46**, 1033–1051 (2011).
57. R. C. Ogliore, G. R. Huss, K. Nagashima, A. L. Butterworth, Z. Gainsforth, J. Stodolna, A. J. Westphal, D. Joswiak, T. Tyliszczak, Incorporation of a Late-Forming Chondrule into Comet Wild 2. *Astrophys. J. Lett.* **745**, L19 (2012).
58. R. C. Ogliore, K. Nagashima, G. R. Huss, A. J. Westphal, Z. Gainsforth, A. L. Butterworth, Oxygen isotopic composition of coarse- and fine-grained material from comet 81P/Wild 2. *Geochim. Cosmochim. Acta* **166**, 74–91 (2015).
59. D. Nakashima, T. Ushikubo, D. J. Joswiak, D. E. Brownlee, G. Matrajt, M. K. Weisberg, M. E. Zolensky, N. T. Kita, Oxygen isotopes in crystalline silicates of comet Wild 2: A comparison of oxygen isotope systematics between Wild 2 particles and chondritic materials. *Earth Planet. Sci. Lett.* **357–358**, 355–365 (2012).
60. C. Defouilloy, D. Nakashima, D. J. Joswiak, D. E. Brownlee, T. J. Tenner, N. T. Kita, Origin of crystalline silicates from Comet 81P/Wild 2: Combined study on their oxygen isotopes and mineral chemistry. *Earth Planet. Sci. Lett.* **465**, 145–154 (2017).

Acknowledgments: We appreciate Prof. Timothy J. Fagan and two anonymous reviewers for their constructive comments. Hayabusa2 was developed and built under the leadership of Japan Aerospace Exploration Agency (JAXA), with contributions from the German Aerospace Center (DLR) and the Centre National d'Études Spatiales (CNES), and in collaboration with NASA, and other universities, institutes, and companies in Japan. The curation system was developed by JAXA in collaboration with companies in Japan. This study is partly supported by JSPS KAKENHI Grant.

Funding: H.Y., T.N., and S.T. acknowledge JSPS KAKENHI Grants.

Author contributions: N.K. and H.Y. designed research; N.K., K.N., N.S., K.B., and T.M. performed research; N.K. and H.Y. analyzed data; and N.K., K.N., N.S., T.M., A.N.K., and H. Y. wrote the paper with contributions from all authors.

Competing interests: The authors declare that they have no competing interests.

Data and materials availability: All data are available in the main text or the supplementary materials.

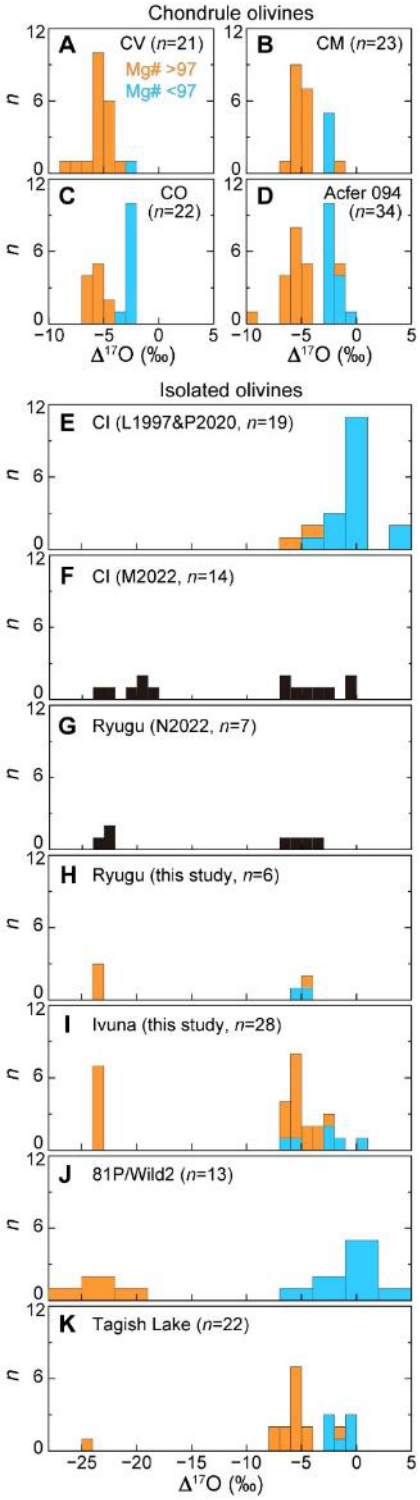

Fig. 1. Histograms of $\Delta^{17}O$ for olivine grains. Chondrule olivine in **(A)** CV chondrite Kaba (*16*), **(B)** CM chondrite Murchison (*15*), **(C)** CO chondrite Yamato 81020 (*14*), and **(D)** ungrouped carbonaceous chondrite Acfer 094 (*13*). Isolated olivine grains in **(E)** CI chondrites Ivuna and Orgueil (previous studies: *4, 6*), **(F)** CI chondrites Ivuna and Alais (previous study: *7*), **(G)** Ryugu (previous study: *8*), **(H)** Ryugu (this study), **(I)** Ivuna (this study), **(J)** comet 81P/Wild2 (*42, 56–60*), and **(K)** ungrouped carbonaceous chondrite Tagish Lake (*49*). Magnesium-rich olivine (Mg# > 97) is shown as orange and Mg-poor olivine (Mg# < 97) in blue, except for (F) and (G) because their chemical compositions are not fully available. Bin sizes of (E) and (J) correspond to their analytical uncertainties. Note that Mg-poor olivine peaks in Yamato 81020 (C) and Acfer 094 (D)

may be enhanced because these studies selectively measured Fe-rich ones from the polished sections. The olivine grains with low $\Delta^{17}O$ are most likely related to refractory inclusions (CAIs and AOAs) while those with high $\Delta^{17}O$ are related to chondrules. L1997=Leshin et al. (1997) [4]; P2020=Piralla et al. (2020) [6]; M2022=Morin et al. (2022) [7]; N2022=Nakamura et al. (2022) [8].

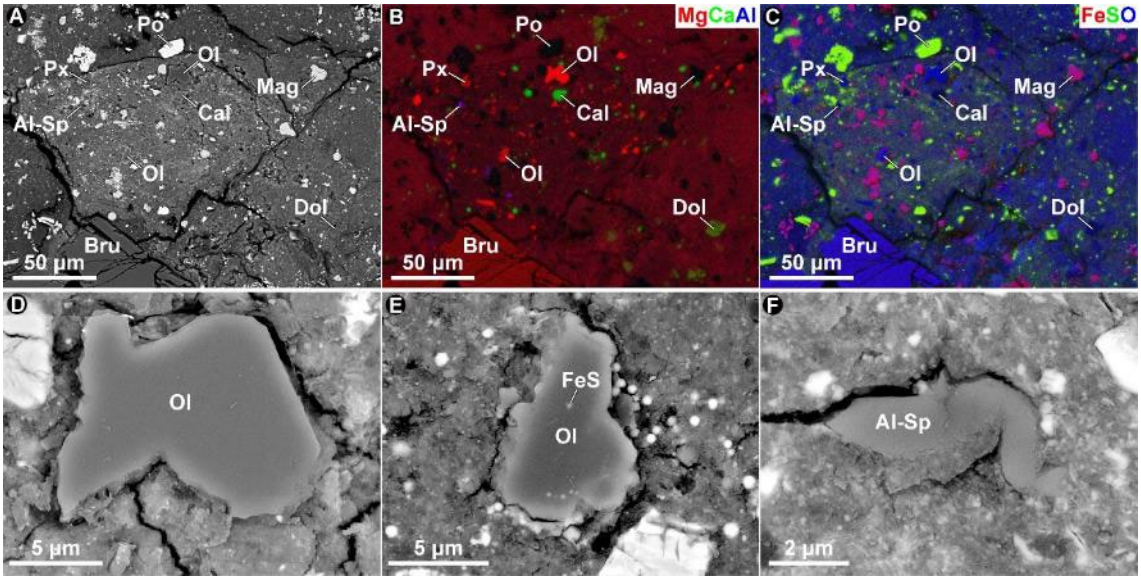

768

769 **Fig. 2. Occurrences of anhydrous primary minerals in Ryugu sample. (A)** Backscattered
770 electron (BSE) image of primary mineral-rich clast. **(B)** Combined X-ray elemental map of (A)
771 using Mg Kα, Ca Kα, and Al Kα lines assigned for RGB channels. **(C)** Combined X-ray elemental
772 map of (A) using Fe Kα, S Kα, and O Kα lines assigned for RGB channels. BSE images of **(D, E)**
773 olivine and **(F)** Mg-Al spinel. The olivine grains (D, E) are located in the clast shown in (A–C).
774 Their O isotopic compositions ($\Delta^{17}O$) are (D) −24‰, (E) −4‰, and (F) −23‰, respectively. Al-
775 Sp: Mg-Al spinel, Bru: breunnerite, Cal: calcite, Dol: dolomite, FeS: Fe-sulfide, Mag: magnetite,
776 Ol: olivine, Po: pyrrhotite, Px: low-Ca pyroxene.
777

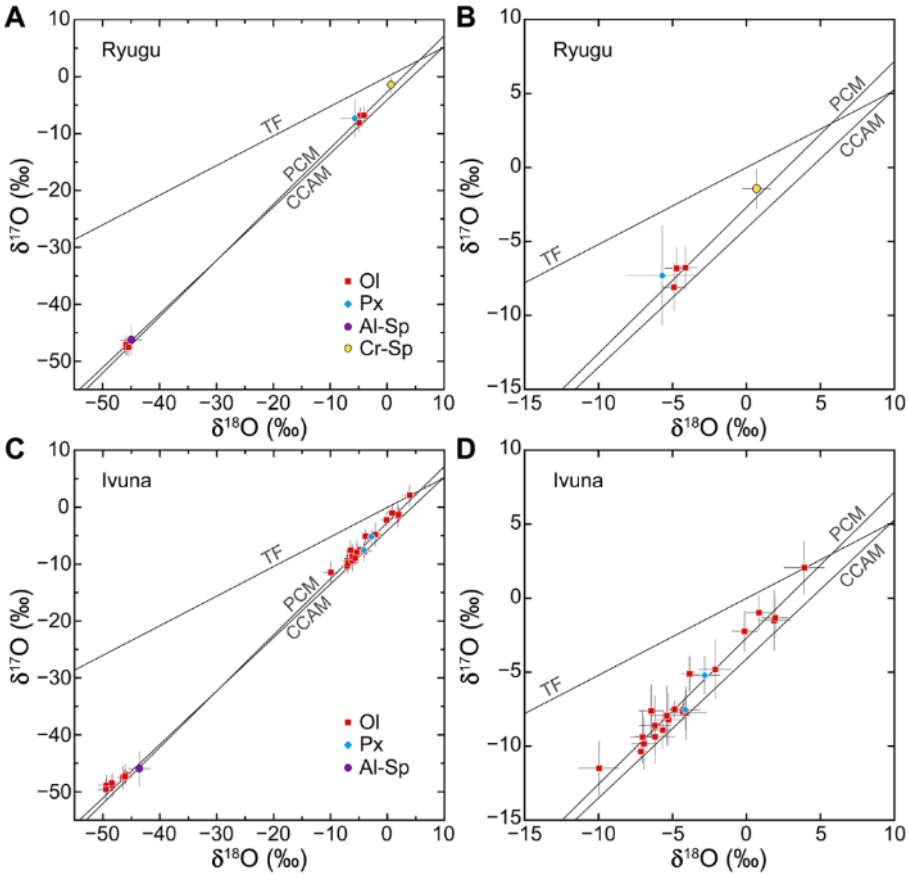

778

779 **Fig. 3. Oxygen isotopic compositions of anhydrous primary minerals. (A, B)** Ryugu. **(C, D)**
780 Ivuna. Data are listed in tables S2, S3 and data S1. Duplicate analyses for each grain showed
781 identical value (within uncertainty of our measurements), suggesting homogeneous O isotopic
782 compositions within grain. Therefore, each point corresponds to a single grain. Errors correspond
783 to 2σ. TF: terrestrial fractionation line, CCAM: carbonaceous chondrite anhydrous mineral line,
784 PCM: primitive chondrule mineral line.
785

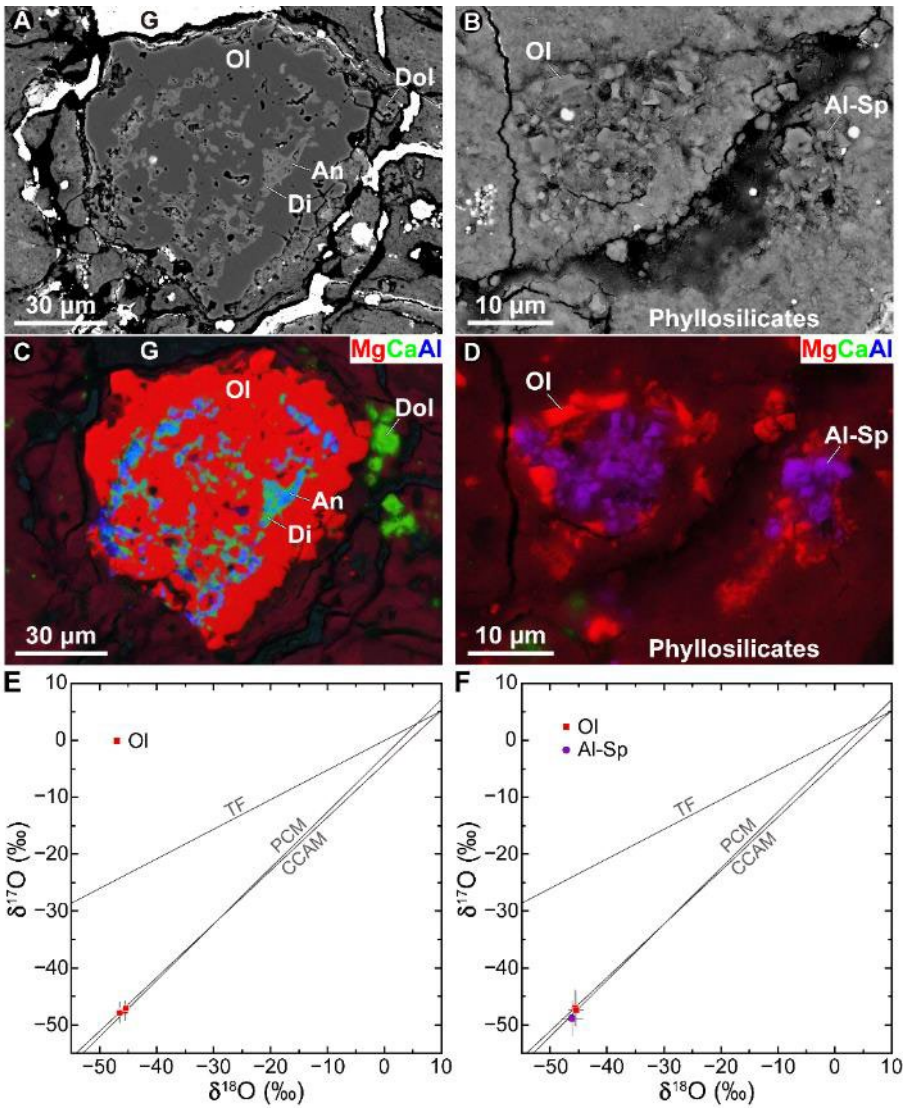

Fig. 4. Refractory inclusions in Ivuna. (A, B) BSE images and **(C, D)** combined X-ray elemental maps of using Mg Kα, Ca Kα, and Al Kα lines assigned for RGB channels of (A, C) amoeboid olivine aggregate (AOA) and (B, D) spinel-olivine inclusion from Ivuna. Oxygen isotopic compositions of individual minerals in **(E)** the AOA and **(F)** the spinel-olivine inclusion. Errors correspond to 2σ. TF: terrestrial fractionation line, CCAM: carbonaceous chondrite anhydrous mineral line, PCM: primitive chondrule mineral line, Al-Sp: Mg-Al spinel, An: anorthite, Di: diopside, Dol: dolomite, Ol: olivine, G: gold coating residue.

Supplementary Materials

Figs. S1 to S51

Tables S1 to S3

Data S1